Romanian Reports in Physics, Vol. 68, No. 3, P. 1240–1258, 2016

ANALYSIS OF SOURCE PROPERTIES FOR THE EARTHQUAKE SEQUENCES IN THE SOUTH-WESTERN CARPATHIANS (ROMANIA)

A.O. PLACINTA, E. POPESCU, F. BORLEANU, M. RADULIAN, M. POPA

National Institute for Earth Physics, P.O. Box MG-2, Calugareni 12, Magurele, 077125, Romania,
E-mail: anca@infp.ro

Received July 7, 2015

Abstract. The crustal seismicity in Romania is concentrated in front of the Carpathians Arc bend (Vrancea region) and at the contact between the extra-Carpathian platform regions and Carpathians orogen. The region investigated in this paper is characterizing the contact of the western side of the South Carpathians with the Tisza-Dacia region. In this area, the large amount of transcurrent deformation that took place during the right-lateral movement of the South Carpathians in respect to the stable Moesian unit let to the creation of intra-mountainous pull-apart basins able to accommodate this movement. For two such basins, Haţeg and Caransebeş-Mehadia, recent good quality seismic data have recorded during three earthquake sequences: (1) a sequence of 14 events occurred on 24–31 March 2011 in the Haţeg Depression (maximum magnitude of M_w = 3.3), (2) a sequence of 35 events occurred on 8–11 September 2013 in the Haţeg Depression (maximum magnitude of M_w = 4.0) and (3) a sequence of 60 events occurred in the Caransebeş-Mehadia Depression on 31 October–15 December 2014 (main shock magnitude of M_w = 4.1). We apply empirical Green's functions deconvolution and spectral ratios techniques to determine the source parameters. Despite the relative small size of the events, high-quality waveforms for pairs of co-located events are available in different measuring sites. The new results, together with previous determinations, provide a useful database to investigate the source scaling properties in correlation with seismotectonics modeling of the study region. Finally, source characteristics (location, seismic moment, source dimension, stress drop, focal mechanism, clustering) are discussed in connection with the seismotectonics features at the scale of the entire Carpathians and adjacent extra-Carpathians contact areas.

Key words: source parameters, source scaling, earthquake sequence, intra-mountain depression, South Carpathians.

1. INTRODUCTION

The area connecting the Balkans with East Carpathians along the highly bended South Carpathians Mountains underwent large-scale strain deformation during Paleocene-Miocene at the contact with Moesia unit (Getic Depression).

Oblique convergence during orogenic subduction and collision is commonly adopted as scenario for the contact between the South Carpathians and Moesia [7]. It implies development of transcurrent zones and creation of pull-apart basins, able to accommodate the large amount of right-lateral movement of the South Carpathians in respect to the stable Moesian unit, driven by the rapid roll-back of a slab attached to the European continent [5, 17, 18].

A few recent earthquake sequences were recorded in the area by the seismic network of the National Institute for Earth Physics (Măgurele, Romania) in two intramountainous depressions characterizing the contact between the South Carpathians and Moesia: Haţeg Depression and Caransebeş-Mehadia Depression (Fig. 1). The two depressions are located at the exterior of the Carpathians, in a region where the largest amount of transcurrent deformation took place and significant amounts of dextral strike-slip deformations were supposed to accommodate the clockwise rotation and N-to-E-ward movement of the Carpathians units in respect to Moesia.

The goal of the paper is to determine the source parameters of these sequences and their scaling and to interpret the results in the context of the main geotectonical features of the region. The sequences were recorded in March 2011 and September 2013 in the Haţeg Depression and in October 2014 in the Caransebeş-Mehadia Depression. The seismicity as recorded in catalogues in the intra-mountain depressions of the East Carpathians is scanty and sporadic. The sequences recently recorded in the Haţeg and Caransebeş-Mehadia depressions are remarkable from this point of view as amount and quality of waveform data.

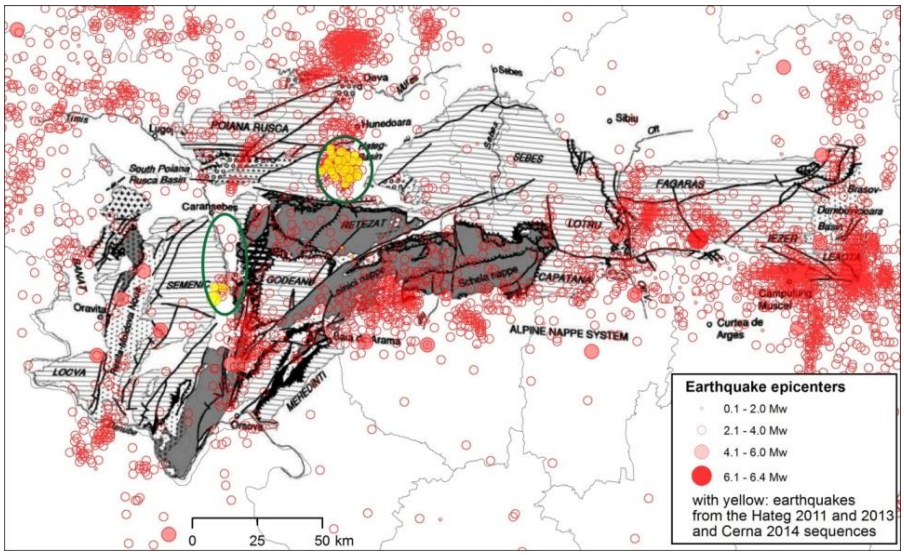

Fig. 1 – Tectonic sketch of the South Carpathians area and associated seismicity (from Romplus catalogue, [11] – updated). Haţeg and Caransebeş-Mehadia depressions are marked by ellipses.

2. REGIONAL SEISMICITY AND TECTONICS

The seismic activity in the study region is generally poor: 69 events with magnitude $M_w \geq 3$ have been recorded since 1900 to the present day (1 June 2015) according to the Romplus catalogue ([11], updated version on www.infp.ro) (Fig. 2). Seismicity concentrates in four clusters related to: (1) Moldova Nouă fault to the west, (2) Cerna fault, (3) Haţeg Depression to the north and (4) the contact between the Getic Depression and the Carpathian orogeny to the east (Fig. 2). Cluster (2) is mentioned as Mehadia-Orşova seismo-active zone by [12]. Cluster (3) is assigned by the same authors as a distinct seismo-active zone. The largest earthquakes were recorded in Moldova Nouă region (a multiple sequence that took place on more than 6-month interval in 1879-1880, with two shocks of M_w = 5.3 and eleven shocks with M_w above 4), Mehadia-Orşova region (an event of M_w = 5.6 recorded in 1991) and Tg.-Jiu region (an event of M_w 5.2 recorded in 1943).

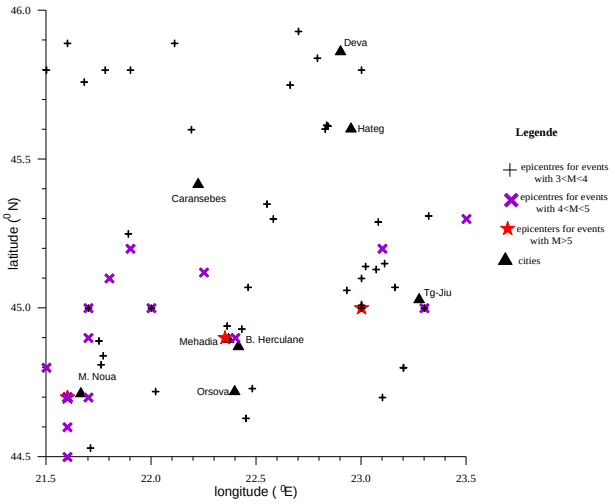

Fig. 2 – Seismicity in the study region ($M_w \geq 3$) as recorded in the Romplus catalogue ([11] – updated).

After 2010 four earthquake sequences took place in the Caransebeş-Mehadia Depression, located north from cluster (2) and in (3) and (4) zones. The sequence in (4) zone was investigated in detail by [15]. Our attention will be focused on Haţeg and Caransebeş-Mehadia zones. In the Haţeg zone two sequences are analysed, one occurred in 24–31 March 2011 (14 events) and the other occurred 8–11 September 2013 (31 events). One earthquake produced rather isolated from the sequence of September 2013, on 31 October 2013, was included in our study taking into account the remarkable proximity of its hypocentre to the sequence hypocentres. The location parameters are given in Table 1 and the epicentre distribution for the two sequences is represented in the Fig. 3. The locations were obtained using the Joint Hypocentre Determination (JHD) algorithm [19].

Table 1

JHD location parameters for the earthquakes occurred in the Haţeg zone

No	yyyy/mo/da	hh:mm:ss	Lat (N^0)	Lon (E^0)	M_L	M_w	h (km)	RMS (s)	No. phas.	GAP
1	*2011/03/24*	*11:02:24*	*45.610*	*22.834*	*3.5*	*3.1*	*3.3**	*.37*	*38*	*60*
2	2011/03/25	02:08:27	45.592	22.832	2.4	2.3	5.5	.27	13	124
3	2011/03/25	02:22:17	45.627	22.746	2.4	2.3	10.8*	.41	9	124
4	2011/03/25	02:29:20	45.598	22.830	2.5	2.4	6.5*	.16	16	121
5	2011/03/25	09:30:53	45.935	22.795	2.5	2.1	5.7	.10	6	142
6	2011/03/25	09:48:58	45.584	22.834	2.5	2.4	7.6	.09	10	123
7	2011/03/25	09:51:12	45.660	22.843	2.4	2.3	9.4*	.19	8	114
8	*2011/03/25*	*12:01:22*	*45.594*	*22.835*	*3.5*	*3.2*	*5.2*	*.35*	*34*	*73*
9	2011/03/25	14:51:26	45.608	22.823	2.5	2.4	5.2	.23	11	120
10	*2011/03/25*	*15:12:24*	*45.602*	*22.827*	*4.0*	*3.3*	*4.8**	*.29*	*37*	*47*
11	2011/03/26	23:37:03	45.594	22.856	2.1	2.2	2.1	.15	8	108
12	2011/03/27	01:13:02	45.639	22.824	2.4	2.3	4.1*	.26	14	101
13	2011/03/27	19:38:30	45.607	22.836	2.2	2.2	4.3*	.31	13	87
14	2011/03/31	06:29:38	45.621	22.841	2.3	2.3	7.5*	.38	13	109
15	*2013/09/08*	*13:00:41*	*45.615*	*22.834*	*4.2*	*3.6*	*5.1**	*.26*	*57*	*43*
16	2013/09/08	13:07:06	45.557	22.856	1.7	2.3	7.4*	.26	11	99
17	2013/09/08	13:07:36	45.611	22.872	1.5	2.2	10.5	.01	6	100
18	2013/09/08	13:09:51	45.628	22.850	0.9	2.0	0.0*	.20	7	110
19	2013/09/08	13:14:52	45.616	22.848	1.7	2.3	5.5	.03	8	88
20	2013/09/08	13:15:48	45.610	22.845	1.0	2.2	8.4	.01	6	101
21	*2013/09/08*	*13:22:11*	*45.612*	*22.840*	*4.7*	*4.0*	*5.6*	*.22*	*83*	*43*
22	2013/09/08	13:27:51	45.608	22.825	1.4	2.2	3.0*	.19	8	100
23	2013/09/08	13:36:50	45.659	22.861	0.5	2.2	0.0*	.21	6	198
24	2013/09/08	13:41:41	45.582	22.816	1.3	2.2	9.3	.01	5	99
25	2013/09/08	13:47:49	45.593	22.800	0.9	2.2	11.8	.02	5	99
26	2013/09/08	14:12:22	45.588	22.836	1.1	2.2	10.4	.01	5	100
27	*2013/09/08*	*14:21:01*	*45.612*	*22.857*	*2.2*	*2.4*	*6.1*	*.21*	*23*	*85*
28	2013/09/08	15:01:39	45.617	22.895	1.0	2.2	0.0*	.30	7	104
29	2013/09/08	15:14:17	45.616	22.837	1.3	2.2	6.4	.02	6	101
30	2013/09/08	15:48:52	45.546	22.931	0.8	2.2	19.6	.03	5	222
31	2013/09/08	16:19:48	45.611	22.835	1.5	2.3	6.4	.17	14	87
32	2013/09/08	16:51:10	45.614	22.837	1.1	2.2	2.2	.05	9	108
33	2013/09/08	17:20:34	45.608	22.844	2.2	2.4	6.4	.17	25	85
34	2013/09/08	18:04:17	45.628	22.854	1.1	2.3	0.0*	.07	7	110
35	2013/09/08	19:51:28	45.610	22.856	1.3	2.3	3.7	.16	14	90
36	2013/09/08	21:09:33	45.596	22.841	0.8	2.2	11.1*	.31	11	90
37	2013/09/08	22:04:00	45.632	22.861	0.7	2.2	0.0*	.46	9	111
38	2013/09/08	22:31:41	45.607	22.851	1.1	2.3	4.9	.25	15	90
39	2013/09/08	23:46:34	45.604	22.841	1.2	2.3	5.2	.07	12	89
40	*2013/09/09*	*15:30:16*	*45.612*	*22.832*	*2.5*	*3.6*	*2.8**	*.40*	*41*	*60*
41	2013/09/09	16:27:17	45.635	22.846	1.1	2.4	6.0	.21	18	85
42	2013/09/09	21:14:40	45.617	22.852	0.7	2.2	2.5	.06	11	101
43	2013/09/10	03:02:55	45.647	22.837	0.8	2.3	8.2	.19	12	88
44	2013/09/11	03:38:57	45.425	22.902	2.2	2.2	23.8*	.21	8	250
45	*2013/10/31*	*06:10:49*	*45.600*	*22.847*	*2.6*	*2.9*	*2.9*	*.37*	*44*	*46*

* location with fixed depth; marked rows: selected events for source parameters evaluation

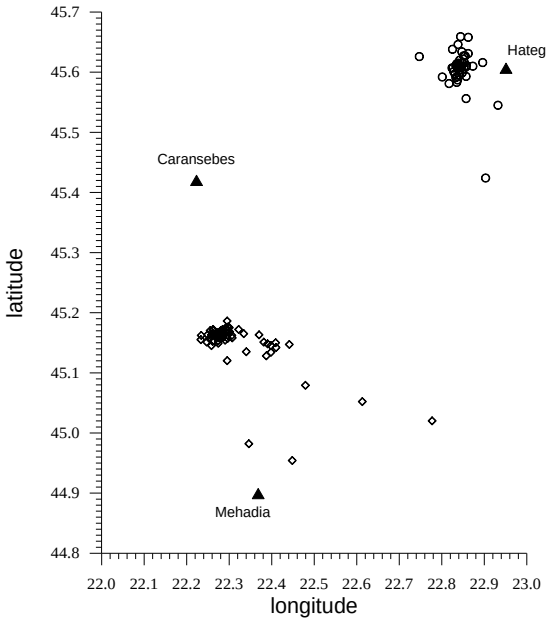

Fig. 3 – Epicentral location of the Haţeg and Caransebeş-Mehadia sequences.

The velocity models adopted in the location procedure correspond with the 1-D structures beneath the closest stations (DEV for Haţeg zone and BZS for Caransebeş-Mehadia zone) as they were determined by [16]. The number of phases used in the location varies from 5 to 83. S-wave phases are picked on the horizontal components. Station covering is satisfactory for the earthquakes in the Haţeg area (GAP is around 100^o as a rule). Except four earthquakes, all the GAP values are below 125^o. The RMS values for the travel time residuals are in all cases below 0.5 s, suggesting relatively well constrained locations. The hypocentral depths are consistently restrained to a 5 to 10 km depth range. The only two outliers (h = 20 km and h = 24 km) are the events with the largest GAPs (222^o and 250^o, respectively).

The sequence of March 2011 has features of a seismic swarm, with three shocks of M_w = 3.2–3.3 and the other shocks of M_w = 1.9–2.4. The sequence of September 2013 has an earthquake of magnitude M_w = 4.0 which distinguishes from the other events as a main shock. It was preceded by 9 foreshocks and followed by 26 aftershocks (including the event of 31 October 2013).

For the Caransebeş-Mehadia zone a sequence running over almost three months is considered (61 events occurred between 31 October 2014 and 6 January 2015). The location parameters are given in Table 2. The epicentre distribution, plotted in the Fig. 3, is roughly E-W elongated. It is noteworthy (Fig. 2) that no earthquake of magnitude above 3 has been ever recorded in the Caransebeş-Mehadia until the event of 31 October 2014.

Table 2

JHD location parameters for the earthquakes occurred in the Caransebeş-Mehadia zone

No	yyyy/mo/da	hh:mm:ss	Lat (°N)	Lon (°E)	M_L	M_w	*h* (km)	RMS (s)	No. phas.	Gap
1	2014/10/31	23:00:03	45.158	22.295	4.7	4.1	7.6	.05	67	58
2	*2014/10/31*	*23:05:39*	*45.162*	*22.274*	*2.4*	*2.5*	*6.2**	*.26*	*27*	*66*
3	*2014/10/31*	*23:08:17*	*45.159*	*22.306*	*1.6*	*1.9*	*6.3*	*.40*	*16*	*58*
4	*2014/10/31*	*23:11:17*	*45.165*	*22.280*	*1.6*	*1.9*	*7.9*	*.09*	*14*	*88*
5	2014/10/31	23:18:47	45.176	22.291	0.7	1.5	.0*	.08	7	106
6	2014/10/31	23:34:11	45.146	22.257	0.8	1.5	.0*	.01	4	159
7	*2014/10/31*	*23:41:04*	*45.173*	*22.261*	*2.5*	*2.7*	*.0**	*.29*	*30*	*66*
8	2014/11/01	00:05:44	45.160	22.276	0.9	1.6	9.5*	.03	8	104
9	2014/11/01	00:08:01	45.165	22.266	1.0	1.6	2.9*	.19	13	102
10	2014/11/01	00:09:45	45.161	22.257	0.6	1.4	.0*	.02	6	102
11	2014/11/01	00:16:32	45.164	22.276	1.1	1.7	8.6	.08	11	104
12	2014/11/01	00:30:12	45.159	22.274	1.2	1.7	11.7	.30	12	88
13	2014/11/01	00:34:40	45.166	22.260	0.7	1.5	.0*	.57	9	101
14	2014/11/01	00:45:18	45.173	22.283	1.3	1.8	5.0*	.15	13	87
15	2014/11/01	01:24:38	45.021	22.776	0.6	1.4	80.7	.23	5	241
16	2014/11/01	01:35:03	45.160	22.285	1.3	1.8	8.0*	.16	14	78
17	2014/11/01	01:42:07	43.558	20.534	2.0	2.1	.0*	.31	8	285
18	2014/11/01	01:45:23	45.173	22.293	1.0	1.6	.0*	.08	6	106
19	2014/11/01	01:51:54	45.155	22.289	2.4	2.4	10.1	.21	11	106
20	2014/11/01	02:14:04	45.187	22.294	0.7	1.5	11	.18	11	107
21	2014/11/01	02:29:58	45.171	22.294	0.5	1.4	.0*	.09	7	107
22	2014/11/01	02:46:12	43.715	20.948	1.5	1.9	4.8	.77	9	280
23	2014/11/01	03:29:02	45.163	22.305	0.9	1.6	13.3*	.35	9	109
24	2014/11/01	04:47:42	45.164	22.257	0.8	1.5	.0*	.21	9	103
25	2014/11/01	05:19:23	45.163	22.233	0.7	1.5	6.5	.04	6	103
26	*2014/11/01*	*05:37:10.*	*45.161*	*22.272*	*1.6*	*1.9*	*7*	*.18*	*16*	*88*
27	*2014/11/01*	*07:16:07*	*45.160*	*22.281*	*1.9*	*2.1*	*8.8*	*.11*	*15*	*87*
28	2014/11/01	09:40:20	44.195	22.100	1.7	2.0	.0*	.37	13	191
29	*2014/11/01*	*12:10:43*	*45.171*	*22.261*	*1.3*	*1.8*	*.0**	*.08*	*8*	*101*
30	2014/11/01	13:48:00	45.168	22.282	1.0	1.6	7	.13	11	87
31	2014/11/01	14:24:21	45.156	22.232	0.7	1.5	8.6	.28	10	96
32	*2014/11/02*	*04:17:30*	*45.162*	*22.280*	*1.9*	*2.1*	*7.1**	*.25*	*25*	*59*
33	*2014/11/02*	*19:39:23*	*45.153*	*22.293*	*2.3*	*2.3*	*0.**	*.46*	*12*	*60*
34	2014/11/02	07:05:30	45.164	22.248	1.1	1.7	1.7*	.21	10	99
35	2014/11/02	23:44:04	45.167	22.279	0.9	1.6	.0*	.09	6	153
36	2014/11/02	23:44:32	45.152	22.246	0.8	1.5	6.9	.08	6	148
37	2014/11/03	03:15:55.	45.159	22.269	1.2	1.7	9	.05	9	146
38	2014/11/04	02:06:57	45.162	22.285	1.3	1.8	8.9	.04	6	145
39	*2014/11/05*	*08:42:15*	*45.150*	*22.273*	*1.6*	*1.9*	*11.8*	*.28*	*8*	*146*
40	2014/11/05	19:52:56	45.176	22.299	1.1	1.7	7.4	.00	5	148
41	2014/11/16	18:52:30	45.168	22.273	1.0	1.6	2.7	.09	7	154
42	*2014/11/18*	*04:27:50*	*45.171*	*22.285*	*1.9*	*2.1*	*4.5*	*.19*	*18*	*69*
43	2014/11/20	03:06:24	45.165	22.279	1.2	1.7	5.3	.12	10	104
44	2014/11/21	10:18:59	45.567	22.410	1.8	2.0	6.1	.47	9	95
45	2014/11/23	16:17:36	45.169	22.300	0.8	1.5	.0*	.14	7	108
46	2014/11/29	07:22:59	45.161	22.276	1.0	1.6	12.7	.33	9	145
47	*2014/12/03*	*10:34:09*	*45.154*	*22.273*	*1.5*	*1.9*	*8.8*	*.18*	*8*	*104*
48	2014/12/06	05:50:50	45.171	22.279	0.9	1.6	.0*	.09	7	152
49	2014/12/10	17:01:45	45.080	22.478	0.9	1.6	50.0*	.71	8	158
50	2014/12/12	09:24:51	46.012	21.901	1.4	1.8	17.3	.21	10	120
51	*2014/12/15*	*09:24:08*	*45.163*	*22.285*	*1.4*	*1.8*	*7.1**	*.16*	*11*	*105*

Table 2

(continued)

No	yyyy/mo/da	hh:mm:ss	Lat (°N)	Lon (°E)	M_L	M_w	*h* (km)	RMS (s)	No. phas.	Gap
52	2014/12/19	23:05:32	45.151	22.408	1.1	1.7	5	.03	9	84
53	2015/01/03	07:49:04	45.053	22.612	0.9	1.6	1.8	.40	9	114
54	2015/01/04	03:27:41	44.983	22.345	1.6	1.9	10.9	.23	15	92
55	2015/01/06	17:35:19	45.152	22.380	1.2	1.7	2.5	.18	10	125
56	2015/01/06	17:46:26	45.149	22.389	1.5	1.9	.0*	.16	9	128
57	2015/01/06	18:14:01	45.146	22.397	1.3	1.8	.0*	.11	9	130
58	2015/01/06	18:16:08	45.164	22.369	1.4	1.8	.0*	.21	10	122
59	2015/01/06	20:14:07	45.143	22.409	0.7	1.5	.0*	.14	6	133
60	2015/01/06	20:18:35	45.148	22.440	0.8	1.5	.0*	.01	4	140
61	2015/01/06	20:52:43	45.135	22.397	0.8	1.5	.0*	.01	4	134

* location with fixed depth
marked rows: selected events for source parameters evaluation

In contrast with the sequences in the Haţeg Depression, the earthquake sequence in the Caransebeş-Mehadia area started clearly with a main event (M_w = 4.1), while all the aftershocks were unusually of small size. The magnitude of the largest aftershock occurred on 31 October 2014 is M_w = 2.7 and the rest of aftershocks have magnitudes less than M_w = 2.5, that means one unit and half less than the mainshock. This behaviour indicates a sudden and efficient energy release from the very beginning of the sequence, followed by a relatively long aftershock effects affecting only low-scale rehabilitation processes.

The fault plane solutions of the events of 24 March 2011, 11:02 (M_w = 3.2), 25 March 2011, 12:01 (M_w = 3.3), 25 March 2011, 15:12 (M_w = 3.2), 8 September 2013, 13:00 (M_w = 3.6) and 8 September 2013, 13:22 (M_w = 4.0), computed using SEISAN algorithm [6] and the first P-wave polarities, are plotted in Fig. 4.

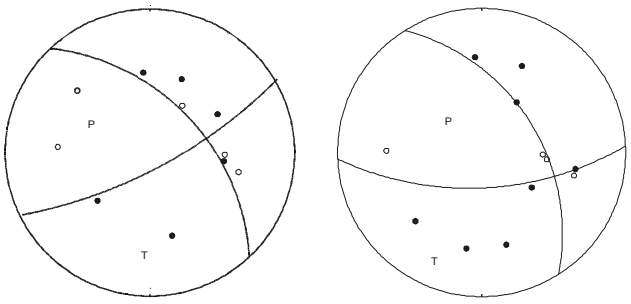

24 March 2011, 11:02 25 March 2011, 12:01

Fig. 4

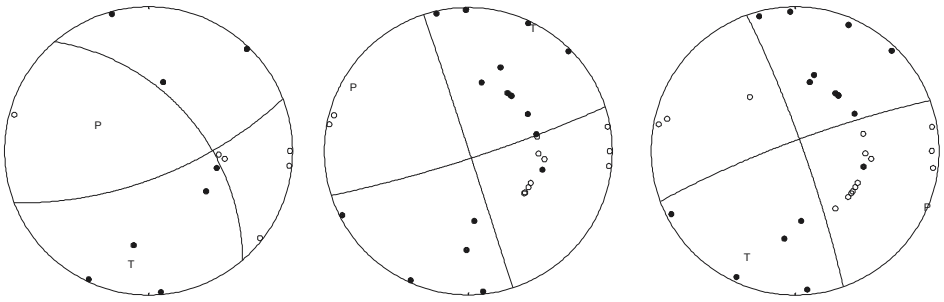

25 March 2011, 15:12 8 September 2013, 13:00 8 September 2013, 13:22

Fig. 4 (continued) – Fault plane solutions for five earthquakes occurred in the Hateg Depression.

The fault plane solutions are close each other with a predominant strike-slip faulting component and principal axes oriented approximately E-W (compression) and N-S (extension). Even if the number of available polarities is small (12–14 polarities for the earthquakes of March 2011), the fault plane solutions are well enough constrained with suitable focal mechanism parameters.

The Haţeg Basin is a postorogenic, intramountainous depression, situated in the north-western part of the Southern Carpathians and represents a former gulf of the Paratethyan realm [13]. Successive fallings inside the basin of the Mesozoic and Tertiary formations were recorded predominantly along NE-SW oriented planes and dipping toward SE. They correspond largely with the nodal planes oriented NE-SW of the fault plane solutions in the Fig. 4. If these nodal planes are adopted as real fault planes, then the focal mechanisms indicate a predominant strike-slip movement with a slight normal faulting: the south-eastern block is falling and north-western block is moving toward NE (dextral movement).

As concerns the earthquake sequence in the Caransebeş-Mehadia Depression, the only reliable fault plane solution can be obtained for the main shock of 31 October 2014 (Fig. 5). The solution obtained using local polarity data is plotted together with the seismic moment tensor solutions determined on regional data by USGS and GFZ (http://www.emsc-csem.org/Earthquake/tensors.php?id=406531&id2=pn907;INFO). Our solution is closer to the USGS than to the GFZ.

The focal mechanisms both in the Haţeg Depression and Caransebeş-Mehadia Depression are compatible with the large-scale transcurrent deformation recorded during the Tertiary drift of the ALCAPA and Tisza–Dacia units into the Carpathians embayment by the rapid roll-back of a slab attached to the European continent [5, 17, 18]. This was coeval with the formation at the interior of the Carpathians of a number of well-studied transtensional to pull-apart basins, such as Haţeg and Caransebeş-Mehadia basins. The largest amount of transcurrent

deformation took place during the right-lateral movement of the South Carpathians in respect to the stable Moesian unit. The clockwise rotation and N- to E-ward movement of the upper Carpathians units in respect to Moesia, were accommodated trough significant amounts of coeval dextral strike-slip deformations ([7] – Fig. 4). The fault plane solutions in Figs. 4 and 5 follow closely this overall pattern if the nodal planes oriented E-W in Haţeg and those oriented NE-SW in Caransebeş-Mehadia experiencing right-lateral movements are considered as real faults.

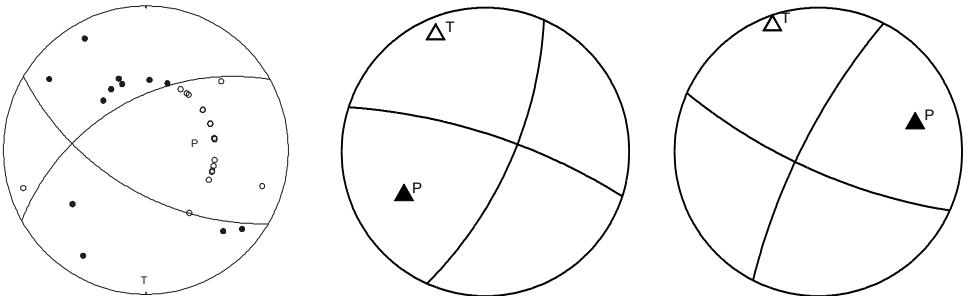

Fig. 5 – Fault plane solution for the main shock generated on October 31, 2014 in the Caransebeş-Mehadia Depression, obtained from local data (polarities) – left, and regional data (waveform inversion) by GFZ and USGS – central and right.

It is interesting to note that the focal mechanism of the 31 October 2014 earthquake resembles the focal mechanism of the M_w = 5.6 earthquake occurred on 18 July 1991 closed to Mehadia, both in terms of principal axes (with a slight difference in the P-axis orientation) and nodal planes [12, 14].

3. SOURCE PARAMETERS USING RELATIVE TECHNIQUES

To constrain the source parameters of the earthquake sequences we applied relative techniques: spectral ratios and empirical Green's function deconvolution. This type of techniques allows path, site and instrument effects removal quite efficiently if we can collect co-located pairs of events recorded by the same instruments at the same sites. An event can approximate the Green's function for a given source – site path if, relative to a larger event, it can be assumed to be the delta function response for that path (empirical Green's function, EGF). In these circumstances, deconvolving EGF from the main event, we remove all propagation effects [10].

For a pair of events, P – principal event and G – Green's function, and for a simple omega-squared source model [4], the spectral ratio is approximated by the theoretical function:

$$R(f) = \frac{\Omega_0^{\,P}\,[1 + (f/f_c^{\,G})^{2\gamma}]^{1/2}}{\Omega_0^{\,G}\,[1+ (f/f_c^{\,P})^{2\gamma}]^{1/2}}\,, \tag{1}$$

where: $\Omega_0^{\,P}$, $\Omega_0^{\,G}$ are the low-frequency plateaus and f_c^P, f_c^G are the corner frequencies of the two events in the pair.

The function that is best fitting the observed spectral ratio is determined iteratively by a nonlinear regression procedure [8]. The free parameters are the ratio of the seismic moments (proportional to the ratio of the low-frequency plateaus of the displacement spectra recorded for the co-located events of the pair) and the corner frequencies (f_c^G –for the Green's event, f_c^P –for the principal event).

The rupture area is directly correlated with the corner frequency [9]:

$$r = k\, v_S/f_c\,, \tag{2}$$

where r is the source equivalent radius, k is a constant (k = 0.32 for P waves and k = = 0.21 for S waves), f_c is the corner frequency and v_S is the velocity of S waves in the focus.

The stress drop value is estimated as a function of seismic moment and source radius [4]:

$$\Delta\sigma = \frac{7M_o}{16r^3}\,. \tag{3}$$

For a given pair P–G events, the corner frequencies f_c^P and f_c^G are estimated from spectral ratio, while the source duration for the P event $\tau_{1/2}$, respectively τ, are estimated from the source time function (STF) resulted after deconvolving the Green's function from the principal event. Subsequently, the source radius can be obtained either from the corner frequency by (2), or from the source duration using [3]:

$$r = (\tau_{1/2} v)/(1–v/\alpha\sin\theta), \tag{4}$$

where $\tau_{1/2}$ is the rise time in the source (for moderate size earthquakes is roughly half of τ), v is the rupture velocity in the source (we adopted in the following v = 0.9β, β – shear wave velocity at focal depth), α –longitudinal wave velocity at source and θ – angle between normal to fault and the emergent angle of the P-wave radiated in the focus.

Practically, for an event considered as principal event (P), we selected a set of associated empirical Green's functions (G events) which are closely located to the respective P event. Then we compute an extended set of spectral ratios and source time functions for all the P – G pairs as recorded at all common stations and taking into account all the three components per station. In principle, the resulted spectral ratios and source time functions depend on source only. Possible differences among stations can result from source directivity effects. These would be detected in correlation with the faulting geometry (higher amplitudes and higher frequencies for the stations situated in front of the rupture direction, while lower amplitudes and lower frequencies for the stations situated in the opposite direction), but such effects were not emphasized for the principal events analyzed in the present work.

The EGF procedure is unstable and the inherent errors could be significant [1]. The shape of the STF is well defined when the P and G events are located nearby, the difference in size between P and G events is sufficiently large (usually at least one unit of magnitude) and the source process is similar in both cases. The filtering is necessary anyway to remove the intrinsic perturbations at high frequencies. The spectral ratios are more robust and are suitable even if the earthquakes in a pair are close in size. But certainly, the procedure requires a useful frequency bandwidth of the sensor as expanded as possible.

Examples of waveforms, spectral ratios and STFs considered for evaluating the source parameters for one pair of events belonging to Haţeg sequence and one pair of events belonging to the Caransebeş-Mehadia sequence are given in Figs. 6 and 7. Only the deconvolutions with well-shaped STFs are selected. Therefore, the number of elements included in the analysis to estimate $< f_c >$ and $< \tau >$ varies from one pair to the other. In the Figs. 8 and 9 we exemplify the averaging procedure applied to obtain the final source parameters.

The dispersion of different values around the average estimations $<f_c>$ and $<\tau>$ shows a relatively narrow range. On the one hand, the seismic moment is computed using:

$$M_0 = (4\pi\rho\alpha^3\Omega_0 R)/R_{\theta\varphi}, \tag{5}$$

where ρ is the density at source, α is the P-wave velocity at source, Ω_o is low-frequency plateau of the displacement spectrum, R is the hypocentral distance, $R_{\theta\varphi}$ is the source radiation factor (we adopted average values, 0.52 for P waves and 0.63 value for S waves, according to [2]. The structural parameters in equation (5) correspond with the model of [16]. On the other hand, the seismic moments are estimated using the spectral ratio level at low frequency (selecting the seismic moment of the principal event as reference):

$$a = \Omega_0^{P}/\Omega_0^{G} = M_0^{P}/ M_0^{G}. \tag{6}$$

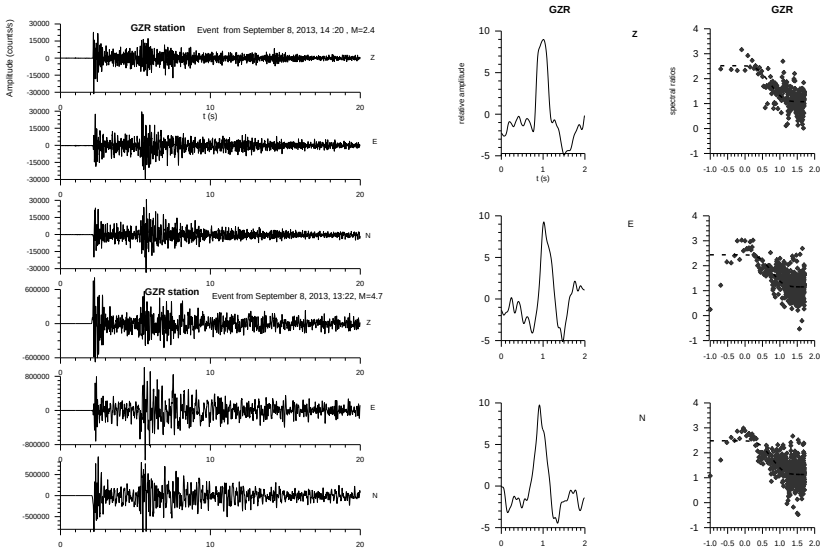

Fig. 6 – An example of pair main event – EGF event for Haţeg Depression to illustrate the procedure applied to determine the source: a) waveforms recorded at GFZ station for event of 8 September 2013, 13:22, $M_w = 4.0$ (main) and of 8 September 2013, 14:21, $M_w = 2.4$ (empirical Green's function); b) the resulted STFs and spectral ratios.

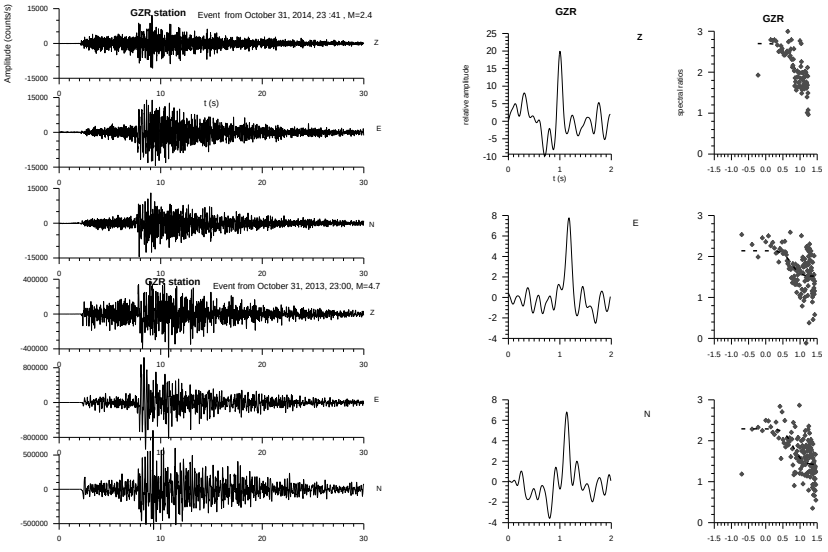

Fig. 7 – An example of pair main event – EGF event for Caransebeş-Mehadia Depression to illustrate the procedure applied to determine the source: a) waveforms recorded at GFZ station for event of 31 October 2014, 23:00, $M_w = 4.1$ (main) and of 31 October 2014, 23:41, $M_w = 2.7$ (empirical Green's function); b) the resulted STFs and spectral ratios.

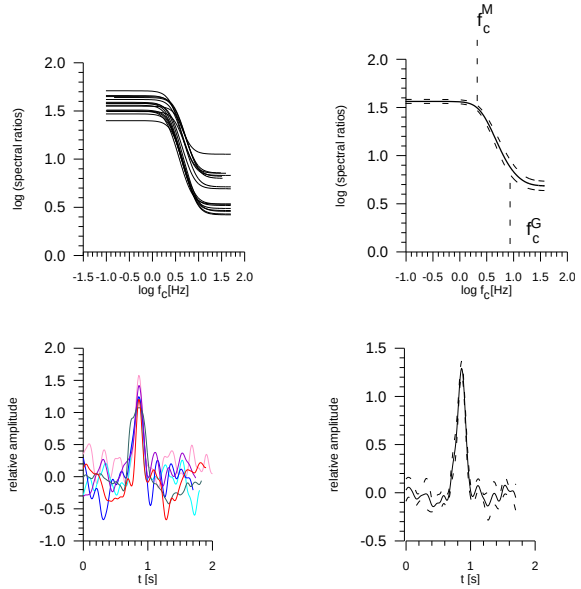

Fig. 8 – Exemplification of the averaging procedure applied to obtain the source parameters from spectral ratios and STFs. Haţeg sequence: main event – 8 September 2013, 13:22, M_w = 4.0; EGF – 31 October 2013, 06:10, M_w = 2.9.

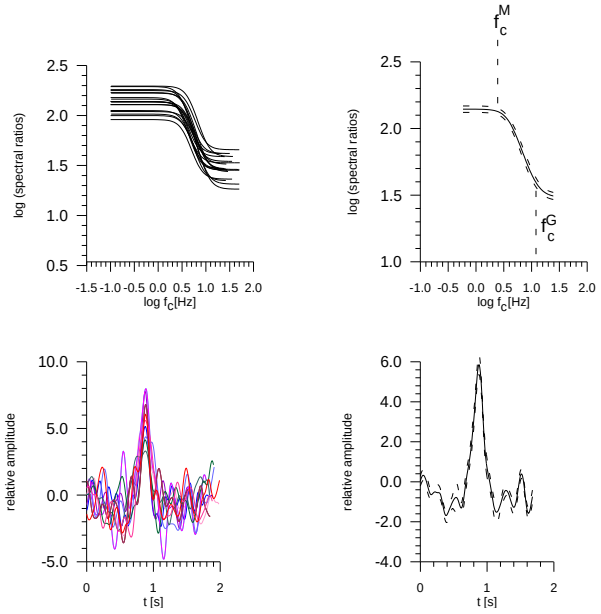

Fig. 9 – Exemplification of the averaging procedure applied to obtain the source parameters from spectral ratios and STFs. Caransebeş-Mehadia sequence: main event – 31 October 2014, 23:00, M_w = 4.0; EGF – 31 October 2014, 23:41, M_w = 2.4.

The earthquakes produced in the Haţeg depression that were selected as principal events are given in Table 3, while the principal events selected for the Caransebeş-Mehadia depression are given in Table 4. Seven earthquakes were selected as EGFs for the principal earthquakes in Table 3 (marked with italic in Table 1). In total, eleven stations were used in analysis: ARR, BANR, BZS, CJR, DEV, DRGR, GZR, LOT, MDVR, SRE, VOIR, each of them with different weight. Thirteen earthquakes were selected as EGFs for the principal earthquakes in Table 4 (marked with italic in Table 2). In total, nine stations were used in analysis: BANR, BZS, CJR, DEV, GZR, LOT, MDVR, SIRR, SRE, each of them with different weight.

Table 3

Haţeg depression: the earthquakes selected as principal events

year/month/day	hh:mm:ss	Lat (N^0)	Lon (^0E)	h (km)	M_w
2011/03/24	11:02:24.75	45.610	22.834	3.0	3.1
2011/03/25	12:01:22.41	45.594	22.835	5.0	3.2
2011/03/25	15:12:24.39	45.602	22.827	5.0	3.3
2013/09/08	13:00:41.96	45.615	22.834	5.1	3.6
2013/09/08	13:22:11.97	45.612	22.840	6.0	4.0
2013/10/31	6:10:49.37	45.600	22.847	3.0	3.0

Table 4

Caransebeş-Mehadia depression: the earthquakes selected as principal events

year/month/day	hh:mm:ss	Lat (N^0)	Lon (^0E)	h (km)	M_w
2014/10/31	23:00:03.13	45.158	22.295	8.0	4.1
2014/10/31	23:05: 39.87	45.162	22.274	6.0	2.5
2014/10/31	23:41: 04.43	45.173	22.261	0.0*	2.7

The final results, obtained after averaging all the particular estimations from spectral ratios and EGF deconvolutions for different P – G pairs recorded at different seismic stations, are presented in Tables 5 (Haţeg) and 6 (Caransebeş – Mehadia).

Table 5a

Source parameters for the main earthquakes in Haţeg Depression

Main event	M_w	M_0 (Nm)	$< f_c >$ (Hz)	$< \tau >$ (s)	r (m)	$\Delta\sigma$ (MPa)
24.03.2011, 11:02	3.1	1.24×10^{14}	7.37	0.1467 ± 0.0229	70	158
25.03.2011, 12:01	3.2	1.06×10^{14}	6.19	0.1629 ± 0.0246	134	19
25.03.2011, 15:12	3.3	1.72×10^{14}	4.33	0.1922 ± 0.0395	120	44
8.09.2013, 13:00	3.6	5.18×10^{14}	3.81	0.2812 ± 0.0418	214	23
8.09.2013, 13:22	4.0	1.87×10^{15}	2.97	0.2921 ± 0.0532	269	42
31.10.2013, 06:10	3.0	7.38×10^{13}	6.94	0.1326 ± 0.0120	75	77

Table 5b

Source parameters for the empirical Green's function earthquakes in Haţeg Depression

EGF event	M_w	M_0 (Nm)	$< f_c >$ (Hz)	r (m)	$\Delta\sigma$ (MPa)
8.09.2013,14:21	2.5	1.37×10^{13}	11.18	73	15
9.09.2013,15:30	2.7	2.44×10^{13}	7.08	98	11

Table 6a

Source parameters for the main earthquakes in Caransebeş-Mehadia Depression

Main event	M_w	M_w (Nm)	$< f_c >$ (Hz)	$< \tau >$ (s)	r (m)	$\Delta\sigma$ (MPa)
31.10.2014, 23:00	4.1	1.94×10^{15}	3.714	$\tau = 0.2457 \pm 0.0457$	228	72
31.10.2014, 23:05	2.5	1.10×10^{13}	10.2	$\tau = 0.1358 \pm 0.0396$	78	10
31.10.2014, 23:41	2.7	2.36×10^{13}	8.28	$\tau = 0.1357 \pm 0.0320$	95	12

Table 6b

Source parameters for the Green's functions earthquakes in Caransebeş-Mehadia Depression

EGF event	M_w	M_0 (Nm)	$< f_c >$ (Hz)	r (m)	$\Delta\sigma$ (MPa)
31.10.2014, 23:08	2.5	8.23×10^{12}	11.93	76	8
31.10.2014, 23:11	2.5	8.55×10^{12}	14.25	65	14
01.11.2014, 05:37	2.4	6.59×10^{12}	11.50	57	–
01.11.2014, 07:16	2.5	8.62×10^{12}	10.35	88	6
01.11.2014, 12:10	2.1	2.04×10^{12}	14.75	62	4
02.11.2014, 04:17	2.2	3.36×10^{12}	12.68	64	6
02.11.2014, 19:39	2.3	4.77×10^{12}	13.30	69	6
05.11.2014, 08:42	2.2	2.95×10^{12}	12.46	74	3
18.11.2014, 04:27	2.4	4.55×10^{12}	12.05	76	5
03.12.2014, 10:34	2.4	5.90×10^{12}	12.48	74	6
15.12.2014, 09:24	2.2	3.16×10^{12}	15.22	54	9

4. SCALING OF THE SOURCE PARAMETERS

Source parameters and their scaling properties are supposed to be indicators of the geotectonic particularities in the region of contact between the South Carpathians and Moesian Platform. As shown by the focal mechanisms, the sequences investigated in this paper follow the general strain partitioning at this contact, manifested as clockwise rotation around Moesian promontory, strike-slip and oblique convergence [7]. The application of spectral ratios and empirical Green's function deconvolution techniques provided source parameters for 22 events recorded in the Haţeg Depresion and Caransebeş-Mehadia Depresion (summarized in the Tables 5 and 6 in the previous section).

The scaling of the moment magnitude as a function of local magnitude (Fig. 10) shows a well-constrained linear dependence over the entire magnitude range investigated in this paper ($1 < M_L < 5$):

$$M_w = (0.50 \pm 0.03)\, M_L + (1.49 \pm 0.08) \qquad (7)$$

$$R = 0.95,\ \sigma = 0.15.$$

According to this regression, the two magnitude scales lead to similar values around magnitude 3, M_w exceeds M_L at lower magnitudes and underestimates M_L at larger magnitudes.

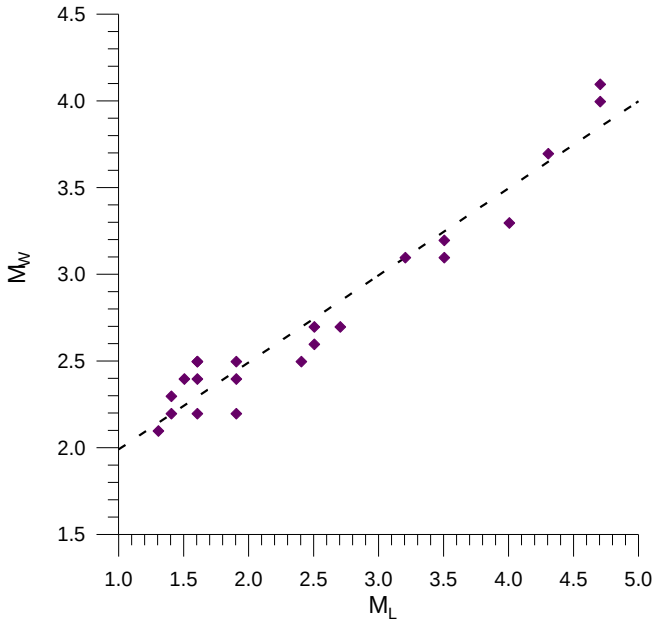

Fig. 10 – Scaling of M_w as function of M_L.

The scaling of the seismic moment with corner frequency is represented in the Fig. 11. The scaling is well approximated by a linear regression:

$$\lg M_o = -(4.04 \pm 0.24) \lg f_c + (17.18 \pm 0.23) \qquad (8)$$

$$R = 0.97,\ \sigma = 0.23.$$

The slope in (8) is greater than the theoretical value (–3) for the scaling of a source with simple rupture process. It is likely that the difference is caused by the underestimation of the corner frequency for the smaller events, taking into account the unavoidable larger errors in the spectral ratios at high frequencies due to noise contribution.

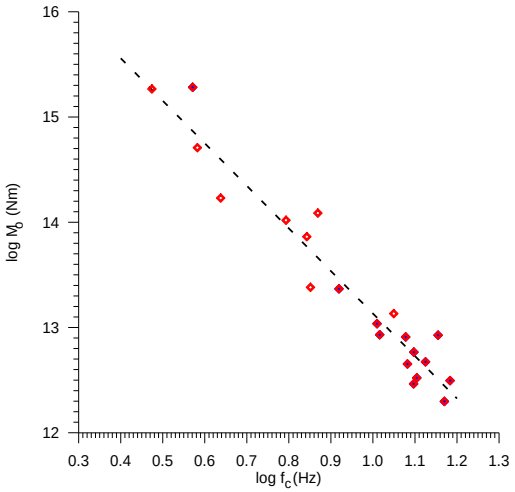

Fig. 11 – Seismic moment *vs* corner frequency.

The scaling of the stress drop versus seismic moment (Fig. 12) apparently shows a non-constant modeling. However, this apparent deviation from constant scaling could be due to two different stress regimes in Haţeg Depression (20–100 MPa) and Caransebeş-Mehadia Depression (5–10 MPa). If we consider the scaling separately on the two regions, a constant scaling is observed for the Haţeg Depression, even if the dispersion of the values is large. In the Caransebeş-Mehadia Depression, a single event has the size comparable with the events in the Haţeg Depression and the associated stress drop fits the same range (close to 100 MPa). All the other events are at least two units of magnitude smaller and the decrease of the stress drop by a factor of 10 could be explained by the underestimation of the corner frequency for the events in this range.

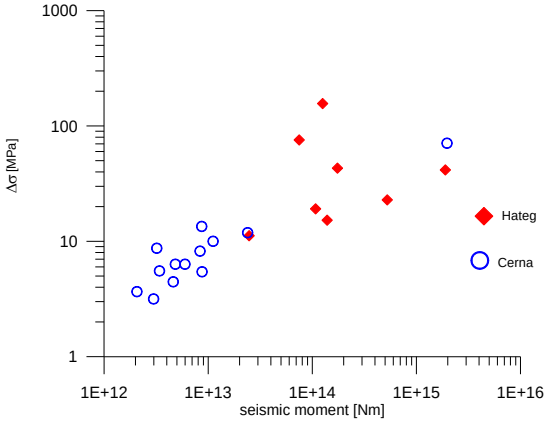

Fig. 12 – Stress drop *vs* seismic moment.

The relatively high stress drop values are compatible with a stress regime specific for intra-continental tectonics. They are in the same range with the stress drop values estimated for the Getic Depression [15].

5. CONCLUSIONS

There are still a lot of questions as regards the way the highly arcuate structure of the South Carpathians was created in the western part of Romania and cross the border, in the north-eastern part of Serbia. The occurrence of three sequences in two of the intra-mountainous depressions characterizing the contact between the South Carpathians and Moesia, Haţeg Depression and Caransebeş-Mehadia Depression, offers an unprecedented opportunity to evaluate reliable source parameters and focal mechanism in this complex geotectonic environment.

Applying spectral ratios technique and empirical Green's function deconvolution we obtain source parameters (seismic moment, source dimension and stress drop) for 23 events belonging to the earthquake sequences occurred on March 2011 and September 2013 in the Haţeg Depression and on October 2014 in the Caransebeş-Mehadia Depression. The epicentral distribution obtain by Joint Hypocenter Determination in correlation with the fault plane solution suggest a predominant dextral strike-slip movement in both depressions, in agreement with the geotectonical modeling of the region [7] which prescribes significant amounts of dextral strike-slip deformations all along the external side of the South Carpathians south-ward bending area able to accommodate the clockwise rotation and N-to-E-ward movement of the Carpathians units in respect to Moesia. The relatively high stress drop values (between 5 to 100 MPa) are compatible with a stress regime specific for intra-continental tectonics. They are in the same range as the stress drop values estimated by [15] for the Getic Depression, located in the inner side of the Carpathians orogenic belt. Note the different deformation field in the last case as shown by the focal mechanisms which is governed by underthrust faulting.

Acknowledgements. This work was partially supported by the project "Nucleu" (PN 09 30/PN09-0104) of the National Plan for Research, Development and Innovation of the Romanian Ministry of National Education and by the Partnership in Priority Areas Program – PNII, under MEN-UEFISCDI, DARING Project no. 69/2014.

REFERENCES

1. R.E. Abercrombie, *Investigating uncertainties in empirical Green's function analysis of earthquake source parameters*, J. Geophys. Res. Solid Earth **120**, doi:10.1002/2015JB011984 (2015).

2. K. Aki, P. Richards, *Quantitative Seismology: theory and methods*, Freeman, San Francisco (1980).
3. J. Boatwright, *A spectral theory for circular seismic sources: simple estimates of source duration, dynamic stress drop, and radiated energy*, Bull. Seismol. Soc. Am. **70**, 1–28 (1980).
4. J.N. Brune, *Tectonic stress and the spectra of seismic shear waves from earthquakes*, J. Geophys.Res. **75**, 4997–5009 (1970).
5. L. Csontos, *Tertiary evolution of the Intracarpathian area: a review*, Acta Vulcanologica **7**, 1–15 (1995).
6. J. Havskov, L. Ottemöller, *SEISAN: The Earthquake Analysis Software*, Version 7.2, University of Bergen, Norway (2001).
7. C. Krézsek, A. Lăpădat, L. Maţenco, K. Arnberger, V. Barbu, R. Olaru, *Strain partitioning atorogenic contacts during rotation, strike-slip and oblique convergence: Paleogene – Early Miocene evolution of the contact between the South Carpathians and Moesia*, Global and Planetary Change **103**, 63–81 (2013).
8. G.T. Lindley, *Source parameters of the 23 April 1992 Joshua Tree, California earthquake, its largest foreshock and aftershocks*, Bull. Seism. Soc. Am. **84**, 1051–1057, 1994.
9. R. Madariaga: *Dynamics of an expanding circular crack*, Bull. Seismol. Soc. Am. **66**, 639–666 (1976).
10. J. Mori, A. Frankel, *Source parameters for small events associated with the 1986 North Palm Springs, California earthquake determined using empirical Green functions*, Bull. Seism. Soc. Am. **80**, 278–285 (1990).
11. M.C. Oncescu, V. Mârza, M. Rizescu, M. Popa, *The Romanian earthquakes catalogue between 984 and 1997*, in: Wenzel, F., Lungu, D. (Eds.), *Vrancea Earthquakes: Tectonics, Hazard and Risk Mitigation*, Kluwer Academic Publishers, (continuously updated), 1999, pp. 43–47.
12. E. Oros, M. Diaconescu, *Recent vs Historical seismicity analysis for Banat Seismic Region (western part of Romania)*, Proceedings of the 5th National Conference on Earthquake Engineering and 1st National Conference on Earthquake Engineering and Seismology" (Ed. Vacareanu R., Ionescu C.), Vol. 1: "Seismology and engineering seismology", Conspress, 2014, pp. 181–189.
13. A. Papp, J. Senes, F. Steininger, *Diskution der Äeouivalente des Badenien in Europa, in Chronostratigraphie und Neostratotypen*, Miozän, Veda, VI, 1978, pp. 55–59, Bratislava.
14. M. Radulian, N. Mândrescu, E. Popescu, A. Utale, G. Panza, *Characterization of Romanian seismic zones*, Pure and Applied Geophysics **157**, 57–77 (2000).
15. M. Radulian, E. Popescu, F. Borleanu, M. Diaconescu, *Source parameters of the December 2011– January 2012 earthquake sequence in Southern Carpathians*, Romania, Tectonophysics **623**, 23–38 (2014).
16. V. Răileanu, D. Tătaru, B. Grecu, *Crustal models in Romania – I. Moesian platform*, Romanian Report Phys. **64**, 539–554 (2012).
17. M. Săndulescu, *Cenozoic tectonic history of the Carpathians*, in Royden, L., Horváth, F. (Eds.), *The Pannonian Basin: a Study in Basin Evolution: AAPG Memoir* **45**, 17–25 (1988).
18. S.M. Schmid, D. Bernoulli, B. Fügenschuh, L. Maţenco, S. Schefer, R. Schuster, M. Tischler, K. Ustaszewski, *The Alpine–Carpathian–Dinaridic orogenic system: correlation and evolution of tectonic units*, Swiss Journal of Geosciences **101**, *1*, 139–183 (2008).
19. Smith, Euan C.G., *An efficient algorithm for routine joint hypocentre determination*, Physics of the Earth and Planetary Interiors **30**, *2–3*, 135–144 (1982).